Acta Oceanol. Sin., 2019, Vol. 38, No. 5, P. 62–75
https://doi.org/10.1007/s13131-019-1440-4
http://www.hyxb.org.cn
E-mail: hyxbe@263.net

Unusual coastal ocean cooling in the northern South China Sea by a katabatic cold jet associated with Typhoon Mujigea (2015)

Yuxin Shi[1], Lingling Xie[1]*, Quanan Zheng[1, 2], Shuwen Zhang[1], Mingming Li[1], Junyi Li[1]

[1] Guangdong Key Laboratory of Coastal Ocean Variation and Disaster Prediction, Guangdong Ocean University, Zhanjiang 524088, China

[2] Department of Atmospheric and Oceanic Science, University of Maryland, College Park, Maryland 20742, USA

Received 16 March 2018; accepted 11 April 2018

Abstract

This study deals with a unusual cooling event after Typhoon Mujigea passed over the northern South China Sea (SCS) in October 2015. We analyze the satellite sea surface temperature (SST) time series from October 3 to 18, 2015 and find that the cooling process in the coastal ocean had two different stages. The first stage occurred immediately after typhoon passage on October 3, and reached a maximum SST drop of –2°C on October 7 as the usual cold wake after typhoon. The second stage or the unusual extended cooling event occurred after 7 d of the typhoon passage, and lasted for 5 d from October 10 to 15. The maximum SST cooling was –4°C and occurred after 12 d of typhoon passage. The mechanism analysis results indicate that after landing and moving northwestward to the Yunnan-Guizhou Plateau (YGP), Typhoon Mujigea (2015) met the westerly wind front on October 5. The low-pressure and positive-vorticity disturbances to the front triggered meridional air flow and low-pressure trough, thus induced a katabatic cold jet downward from the Qinghai-Tibet Plateau (QTP) passing through the YGP to the northwestern SCS. The second cooling reached the maximum SST drop 4 d later after the maximum air temperature drop of –9°C on October 11. The simultaneous air temperature and SST observations at three coastal stations reveal that it is this katabatic cold jet intrusion to lead the unusual SST cooling event.

Key words: Typhoon Mujigea (2015), second-round cooling, katabatic cold jet, South China Sea, westerly wind front

Citation: Shi Yuxin, Xie Lingling, Zheng Quanan, Zhang Shuwen, Li Mingming, Li Junyi. 2019. Unusual coastal ocean cooling in the northern South China Sea by a katabatic cold jet associated with Typhoon Mujigea (2015). Acta Oceanologica Sinica, 38(5): 62–75, doi: 10.1007/s13131-019-1440-4

1 Introduction

Typhoon is severe atmospheric vortex movement, occurring frequently in low and middle latitudes. Typhoon landing brings strong winds, rainstorms, and storm surges, which may cause severe disasters and damages to lives and properties in the coastal regions. Sea surface temperature (SST), a basic parameter of the ocean, plays an important role in the strong air-sea interaction during the typhoon process (Cione and Uhlhorn, 2003; Webster et al., 2005; Yang and Hou, 2014; Lin and Chan, 2015; Glenn et al., 2016; Wang et al., 2017). Therefore, SST response to typhoon has attracted much attention of researchers in recent decades (Price, 1981; Wentz et al., 2000; Zheng et al., 2006; Price et al., 2008; Zhang et al., 2014; Allahdadi and Li, 2018).

The typhoon passage usually induces the SST drop in the open ocean (Price, 1981; Walker et al., 2005; D'Asaro et al., 2007; Shan et al., 2014; Zhang et al., 2016). The SST drop ranges from less than –1°C up to –11°C (Lin et al., 2003; Zheng et al., 2010; Chiang et al., 2011). The maximum cooling mostly appears on the right side of the typhoon track (Nelson, 1996; Black and Dickey, 2008). Dare and McBride (2011) analyzed SST response to typhoon in the global oceans from 1981 to 2008. They found the maximum SST cooling occurred between Day –1 to Day +7 relative to the typhoon passage with the most common occurrence of 1 d after typhoon passage. Xu and Su (2007) analyzed SST response to typhoon in the northwestern Pacific from 2001 to 2005. They found that the maximum SST cooling mostly occurred 2 or 3 d after typhoon passage. It usually takes several days to weeks for recovery, except that accelerated by advection of warm water (Yang et al., 2012b; D'Asaro et al., 2014; Liu et al., 2017). The storm intensity and the translation speed affect the degree of SST response and the recovery time (Price, 1981; Cione and Uhlhorn, 2003; Tsai et al., 2008). In the coastal ocean, the SST drop seems to be less related to the typhoon intensity (Xu and Su, 2007; Xie et al., 2017). The maximum SST drop can also appear on the left side of the typhoon track (Kuo et al., 2014; Lai et al., 2013). The maximum SST drop generally occurs 1 or 2 d after typhoon passage and recovers quickly 3–5 d later (Liang and Ge, 2014), faster than that in the deep ocean (Yang et al., 2012a; D'Asaro et al., 2014). Typhoon not only causes cooling but also warming in the coastal ocean, and the incidence angle of typhoon with respect to the shelf is an important factor affecting SST response as well (Pan and Sun, 2012; Tsai et al., 2012; Xie et al., 2017).

Foundation item: Foundation item: The National Natural Science Foundation of China under contract Nos 41776034, 41476009 and 41706025; the GASI Project under contract Nos GASI-IPOVAI-01-02 and GASI-02-SCS-YGST2-02; the Natural Key Research and Development Program of China under contract No 2016YFC1401403; the Foundation of Guangdong Province for Outstanding Young Teachers in University under contract No. YQ201588.
*Corresponding author, E-mail: llingxie@163.com

The northern South China Sea (SCS) is an area where the typhoons pass frequently (Wang et al., 2007). The SST drop after typhoon passage has been investigated by previous investigators (Shang et al., 2008; Zheng et al., 2008; Pan and Sun, 2012; Yang et al., 2012a or b?; Zhang et al., 2014; Liu et al., 2014). However, a second-round SST drop after recovery of the first maximum SST drop has seldom reported. Typhoon Mujigea (2015) was a super-typhoon occurred in October 2015. It passed through the northern SCS and landed at Zhanjiang, China on October 3–4, 2015. The coastal ocean SST decreased to a maximum cooling of –2°C on October 7 after 3 d of Mujigea passage (Shi et al., 2017). The SST warmed up on October 8, while a following second-round cooling occurred on October 10 after 7 d of typhoon passage. The maximum cooling reached –4°C and lasted for 5 d, stronger than the first cooling event on October 7. This study reports this unusual second-round cooling event, and aims to reveal the mechanism for the second cooling event further.

This paper is organized as follows: the next section introduces typhoon Mujigea (2015) and datasets used for this study. Section 3 describes the extended cooling event induced by the typhoon. The SST variability at three offshore stations is quantitatively analyzed. Section 4 analyzes the atmospheric and oceanic mechanisms probably affecting the extended SST cooling on the basis of heat budget equation. Section 5 examines the dynamics of interaction of typhoon with the large-scale atmospheric circulation to induce the unusual ocean cooling. Sections 6 and 7 contain the discussion and conclusions, respectively.

2 Data and methodology

2.1 *Data sources*

2.1.1 *Typhoon and wind*

The typhoon data used in this study are downloaded from the Typhoon Database of the Joint Typhoon Warning Center (JTWC), including every 6 h typhoon intensity, center position, center minimum pressure, and maximum wind speed (http://weather.unisys.com/hurricane/w_pacific/2015/index.php/).

The sea surface wind data are ASCAT surface wind data products downloaded from ftp://ftp.ifremer.fr/ifremer/cersat/products/gridded/mwf-ascat/data/daily/Netcdf/2015/. The spatial resolution is 0.25°×0.25°. The temporal resolution is 1 d.

2.1.2 *Air temperature, precipitation and geopotential height*

The air temperature at 2 m and the precipitation data are downloaded from the ERA-Interim provided by European Center for Medium-Range Weather Forecasts (ECMWF) (http://apps.ecmwf.int/datasets/data/interim-full-daily/levtype=sfc/). The spatial resolution is 0.125°×0.125°.The temporal resolution is 6 and 12 h, respectively. The 500 hPa geopotential height data are the NCEP-DOE reanalysis data provided by the Earth System Research Laboratory (ESRL) (http://www.esrl.noaa.gov/psd/data/gridded/data.ncep.reanalysis2.pressure.html). The spatial resolution is 2.5°×2.5°. The temporal resolution is 1 d.

2.1.3 *SST, SSHA and sea surface current*

The SST data are downloaded from the UK Meteorological Office (UKMO) (http://data.nodc.noaa.gov/ghrsst/L4/GLOB/UKMO/OSTIA/2015/). The spatial resolution is 0.125°×0.125°, and the temporal resolution is 1 d.

The sea surface height anomaly (SSHA) data are downloaded from AVISO (http://www.aviso.altimetry.fr/en/data/data-access/gridded-data-extraction-tool.html), which are merged by multiple satellite data. The spatial and temporal resolutions are 0.25°×0.25° and 1 d, respectively.

The sea surface current data are derived from the simple ocean data assimilation (SODA) dataset developed by the University of Maryland, College Park, Maryland, USA (http://www.atmos.umd.edu/~ocean/index_files/soda3.3.1_mn_download.htm). The spatial resolution is 0.25°×0.25°. The temporal resolution is 5 d.

2.1.4 *Surface heat flux*

Surface heat flux data are downloaded from the ERA-Interim provided by European Center for Medium-Range Weather Forecasts (ECMWF) (http://apps.ecmwf.int/datasets/data/interim-full-daily/levtype=sfc/). The data include surface net solar radiation, surface net thermal radiation, surface sensible heat flux and surface latent heat flux. The spatial resolution is 0.125°×0.125°. The temporal resolution is 12 h.

2.2 *Study area and Typhoon Mujigea (2015)*

The study area is the northwestern continental shelf of the SCS ranging from 18° to 23°N and from 109° to 115°E. The Typhoon Mujigea (2015) was generated in the Pacific at 2:00 UTC on October 2, 2015, and moved northwestward. After entering the SCS, its intensity was continuously strengthened. It became a tropical storm at 20:00 on October 2, and entered the study area at 14:00 on October 3. As shown in Fig. 1, Mujigea (2015) developed to be a strong typhoon at 18:00 on October 3, with the maximum wind speed of 48 m/s. The gale circle had a radius of 100 km, covering the northwestern SCS. After stayed in the study area for one day, the typhoon landed at Zhanjiang, China at 14:00 on October 4. The radius of the wind circle reduced, but the maximum wind speed strengthened to 57 m/s. It weakened to a strong tropical storm at 18:00 on October 4, moved northwestward faster to the inland, and continued to weaken to a tropical storm at 15:00 on October 5.

3 Extended impact of Typhoon Mujigea (2015) on SST in the northwestern SCS

Figure 2 shows a time series of the SST anomaly (ΔSST) in the

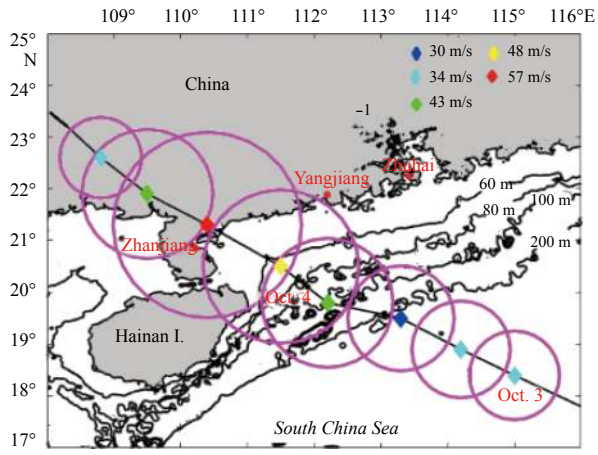

Fig. 1. Track of Typhoon Mujigea (2015) and bottom topography of the northwestern continental shelf of the SCS. Black fold line with magenta circles represents the typhoon track with the range of gale wind. Color diamonds represent the maximum wind speeds. The ocean bottom topographic data are from ETOPO1 (http://maps.ngdc.noaa.gov/viewers/wcs-client/). Isobaths are in m.

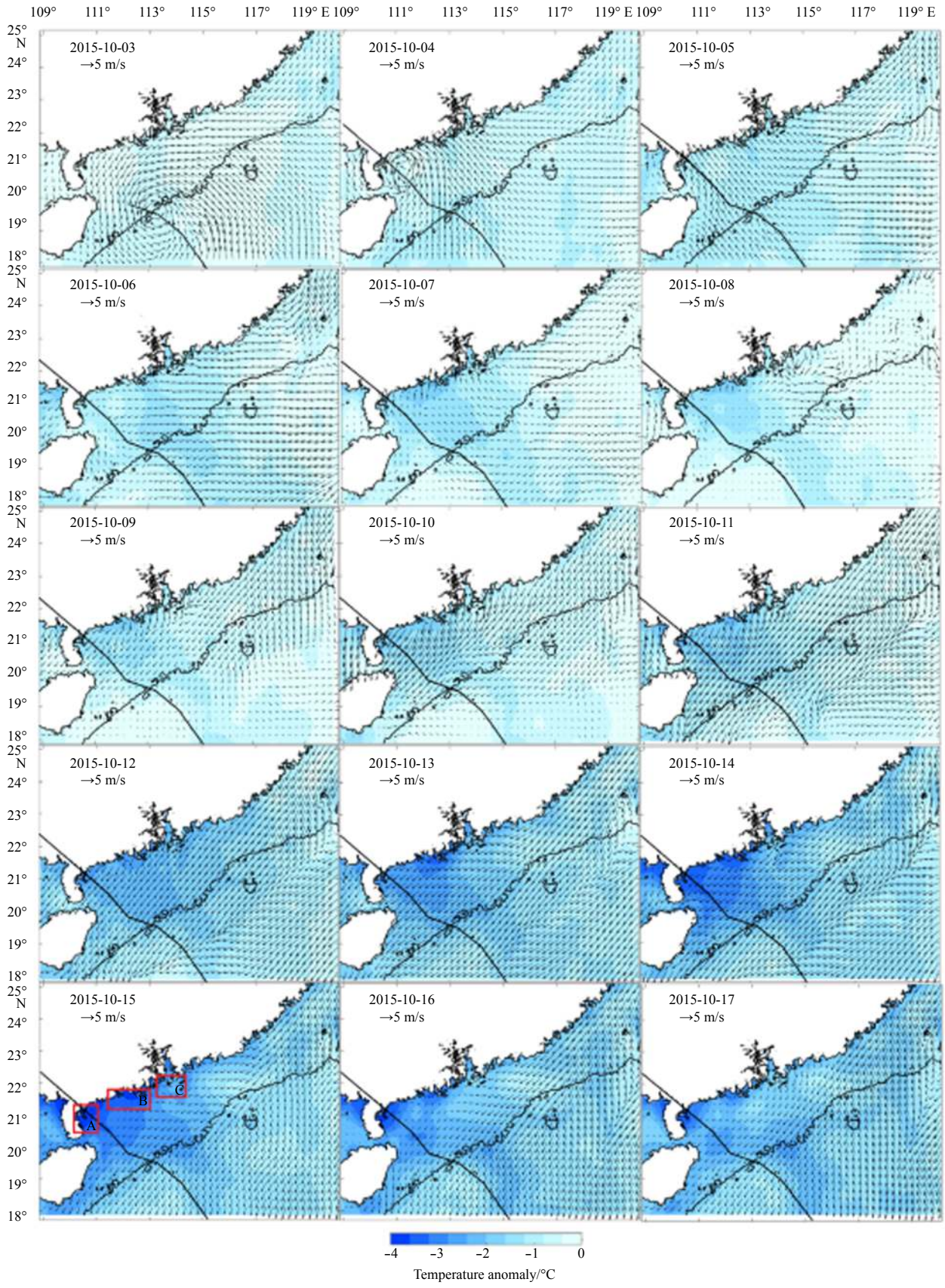

Fig. 2. Time series images of ΔSST and sea surface wind in the northwestern SCS after the Typhoon Mujigea (2015) passage. Black lines represent the typhoon track. Black contours are isobaths of 200 m. Dates of images read year-month-day. Red boxes A, B and C are three offshore test stations near Zhanjiang, Yangjiang and Zhujiang River Estuary, respectively.

northwestern SCS and the corresponding wind field during Typhoon Mujigea (2015) passage. ΔSST is calculated as the daily SST minus the average SST of 7 d from September 26 to October 2 before the typhoon entering the northwestern SCS. One can see that Mujigea entered into the study area on October 3, when its center was located near the 200-m isobath. The SST was cooler in the most area and had a maximum ΔSST of –1°C west of the Zhujiang (Pearl) River Estuary. On October 4, the typhoon center approached the Leizhou Peninsula. ΔSST increased on the right side of typhoon track. On October 5, the northwestern SCS continued to cool down. On October 7, the maximum SST drop reached –2°C. During this period, the sea surface wind changed from the southeasterly wind to the easterly wind, and the wind speeds weakened. The SST began to rebound on October 8. So far, the first cooling stage ended with a maximum ΔSST of –2°C occurred 4 d after typhoon passage. The lag time of the first SST cooling is consistent with previous statistical results (Xu and Su, 2007).

This study focuses on examination of second round of SST drop started on October 10, i.e., the extended cooling event. On the following days, the magnitude and coverage of the negative ΔSST strengthened and spread from the coast to the offshore water. ΔSST reached the maximum value of –4°C near the Leizhou Peninsula on October 15. The study area returned to warming up from October 16 to 17, i.e., the extended cooling lasted for 5 d from October 10 to15.The maximum SST drop was about –4°C on October 15, 12 d after the typhoon passage on October 3. The whole extended cooling process was accompanied by northeasterly wind, which appeared on October 9, reached the maximum wind speed of 15 m/s on October 10–11, and then weakened till October 17.

In order to further understand the extended cooling process, we select three offshore test Stations A–C, where the largest ΔSSTs appeared, for the quantitative analysis. As shown in Fig. 2, Station A is located near Zhanjiang, B near Yangjiang, and C near the Zhujiang River Estuary. The time series of the spatial mean SST anomaly ΔSST_m at the stations are shown in Fig. 3. One can see a similar declined trend at three stations. We further divide the cooling process into two stages. The first stage occurred from October 3 to 7. The second stage, i.e., the extending cooling stage, occurred from October 10 to 15. Between the two cooling stages, there was a recovery period of about 3 d from October 7 to 10. At the first stage, ΔSST_m declined continuously from –0.2°C to a maximum of –1.5°C at Station A (black line), from –0.5°C to –1.7°C at Station B (blue line), and from –0.5°C to –1.1°C at Station C (red line), respectively. The maximum cooling occurred on October 6 at Station C, one day earlier than that at Stations A and B, and lagged the typhoon passage for 3 d. Then, ΔSST_m at three stations rose on October 8 in the recovery period. The rebound at Station C is the most remarkable with ΔSST_{mC} reached –0.7°C on October 9. However, ΔSST_m declined again on October 10 at the second stage. The maximum ΔSST_m reached –3.6°C, –3.3°C and –2.5°C on October 15 at Stations A, B and C, respectively. The second cooling stage was much stronger than the first stage at all three stations, with the maximum SST drops twice of that at the first stage.

The three-day recovery period between the two cooling stages implies the following possibilities. (1) The first cooling stage and the second one are independent events with different mechanisms. (2) Without the second cooling event, the ocean SST would recover to the normal state after the first cooling event. (3) The second cooling event originates from a remote rather than a local location, so that it needs a couple of days to return to the SCS after the first cooling event.

4 Analysis of causes of extended cooling

The decline of SST results from the ocean heat loss, which can be calculated from the heat budget equation of the ocean surface in the form of (Stewart, 2008)

$$Q_t = Q_{sw} + Q_{lw} + Q_L + Q_s + Q_{adv}, \quad (1)$$

where Q_{sw} is the solar short-wave radiation, Q_{lw} is the net long-wave radiation, Q_L is the latent heat, Q_s is the sensible heat, and Q_{adv} is the ocean advection (Stewart, 2008). Ignoring the radiation variation, the heat loss in the study area may be attributed to the atmospheric processes such as wind, precipitation and cold air, which affect the latent and sensible heat fluxes Q_L and Q_s, and the ocean dynamic processes such as cold flow and cold vortex associated with the advection Q_{adv}. In the case of extended cooling, the effects of these factors will be analyzed as follows.

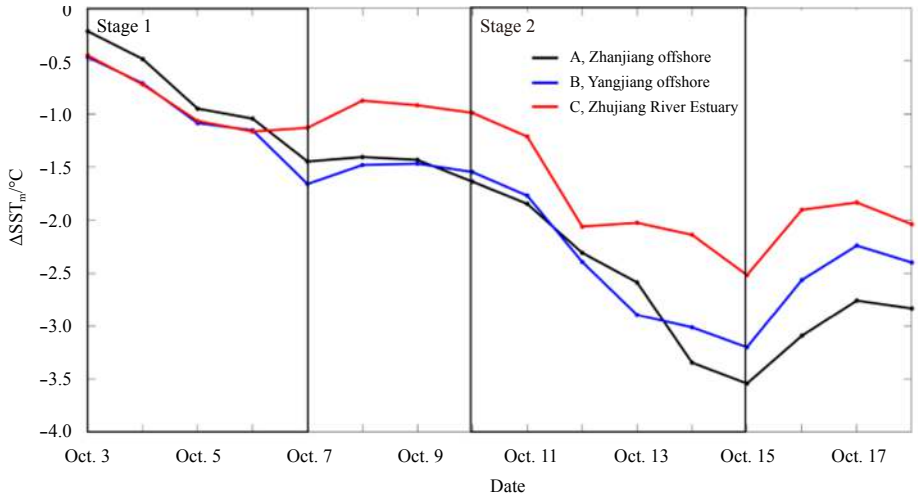

Fig. 3. Variability of the region-averaged ΔSST_m (°C) at Stations A, B and C as shown in Fig. 2. Two black boxes represent the first cooling stage and the extended cooling stage, respectively.

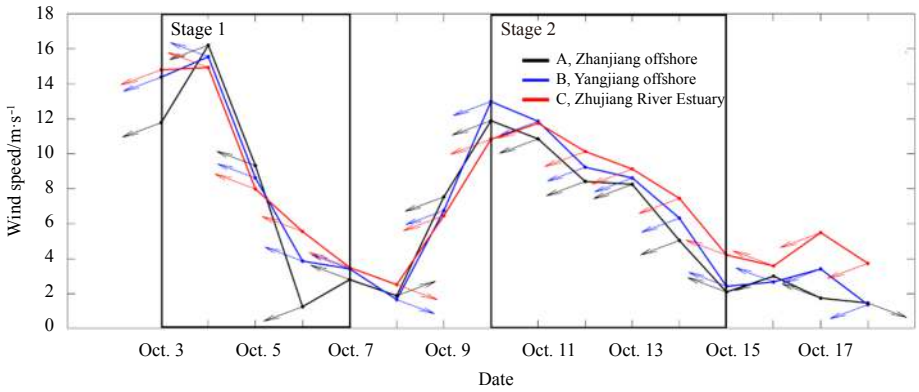

Fig. 4. Variability of the region-averaged sea surface wind speeds at Stations A, B and C. Arrows represent the wind direction.

4.1 *Sea surface winds*

Figure 4 shows variation of the averaged wind vector at Stations A-C. One can see that the southeasterly winds were prevailed during the first cooling stage from October 3 to 7, consistent with the wind field shown in Fig. 2. The maximum speed was 16 m/s occurred on October 4, when Typhoon Mujigea (2015) landed. The wind speed decreased to about 2 m/s on October 8, and then dramatically increased to 12 m/s on October 11 with the wind direction changing to northeasterly from October 9. At the extended cooling stage from October 10 to 15, northeasterly winds controlled the coastal ocean. However, the wind speeds decreased from a maximum of 13 m/s on October 10 to a minimum of 2 m/s on October 15 at Stations A and B, and one day later at Station C. Comparing the variability of wind speed to that of the SST drop, one can see that the wind speed decreased as ΔSST_m enhanced at the extended cooling stage. The correlation coefficients between the wind speed and the minus values of ΔSST_m are 0.98, 0.92 and 0.84 at Stations A, B and C, respectively.

According to Eq. (1), the sea surface heat loss should be out of phase with the wind speed decrease, i.e., negatively correlated. The above positive correlation coefficients and the northward and seaward spread of the SST cooling shown in Fig. 2 imply that the weakened northeasterly wind should not be related to the extended cooling, but the two accompanied processes are controlled together by large-scale atmospheric circulation system.

4.2 *Precipitation*

Figure 5 shows the precipitation process in the study area after Mujigea (2015) passage. One can see that the precipitation centers were located on the both side of the typhoon track on October 3. The maximum precipitation rate reached 20 mm/d. On October 4, the precipitation center was located on the right side of the typhoon track. The maximum precipitation rate reached 18 mm/d. On October 5, after the typhoon landing, the precipitation decreased and the maximum participation rate of 6 mm/d appeared in the coastal ocean of western Guangdong, China. On October 6, the precipitation centers moved to Hainan Island and the Zhujiang River Estuary with the maximum precipitation rate of 5 mm/d and 6 mm/d, respectively. On October 7, the precipitation continued decreasing with the maximum rate of 4 mm/d. After October 10, a new precipitation process appeared around the Hainan Island but moved southward out of the study area on October 15. On the other hand, the extended cooling area rapidly expanded from the coastal ocean on October 11 to the slope waters near 200 m isobaths on October 15. From the above analysis, we find an important fact, i.e., the development process of precipitation did not coincide with that of the extended cooling. This means that precipitation is not a decisive factor to form the SST distribution patterns at the extended cooling stage. Therefore, we need to continue the search for other processes, which are significant for the extended cooling.

4.3 *Air temperature*

Besides the wind and precipitation, the air temperature is an important factor directly affecting the sea surface heat flux. Figure 6 shows the time series weather charts of the 2-m temperature anomaly, i.e., ΔT_{2M}, and the potential heights at 500 hPa after Mujigea (2015) passage. ΔT_{2M} is calculated as the daily 2-m air temperature minus that an average value between September 26 and October 2 before Mujigea (2015) entering the northwestern SCS. One can see that the low-pressure center of the typhoon landed over the Leizhou Peninsula on October 4. In the northern coverage of the typhoon, the air temperature dropped with ΔT_{2M} of about –2°C. On October 5, the low center reached the Yunnan-Guizhou Plateau (YGP) and ΔT_{2m} decreased dramatically to –5°C. On October 6, the typhoon center weakened but a meridional low-temperature disturbance band still existed in the zonally-distributed potential height contours. On October 7, a katabatic cold jet from Qinghai-Tibet Plateau (QTP) developed along the trough between the Yunnan Plateau and the Guizhou Plateau. The cold jet intensified and rapidly intruded southwestward to the coastal area near the Beibu Gulf on October 9. On October 10, the cold air expanded both southward and eastward, covered the Beibu Gulf and reached the Guangdong coastal area. The cold air continually intruded southward to cover the northwestern SCS on October 11. The maximum ΔT_{2M} reached –10°C. The cold air over the coastal ocean faded on October 12, and the temperature inland warmed up after October 13.

We further calculate the time series of regional mean of air temperature anomaly, i.e., ΔT_{2Mm}, at Stations A–C. The results are shown in Fig. 7. One can see that the trends of the air temperature variability are very close, i.e., the biggest drop occurred on October 11 at the second cooling stage. The maximum drop of ΔT_{2Mm} was –9°C, –8.5°C and –7.8°C, respectively. Comparing Figs 3 and 7, one can see that variations of air temperature and SST are in good agreement. ΔT_{2Mm} increased on October 8 and 9, and the SST had a corresponding recovery period between the two cooling stages, implying the effect of air temperature on SST variation. $\Delta T_{2Mm}$was the lowest at Station C, and the SST drop was the lowest as well. In addition, ΔT_{2Mm} at the stations simultaneously reached the maximum drop on October 11, while SST simultaneously reaching the maximum drop on October 15, i.e.,

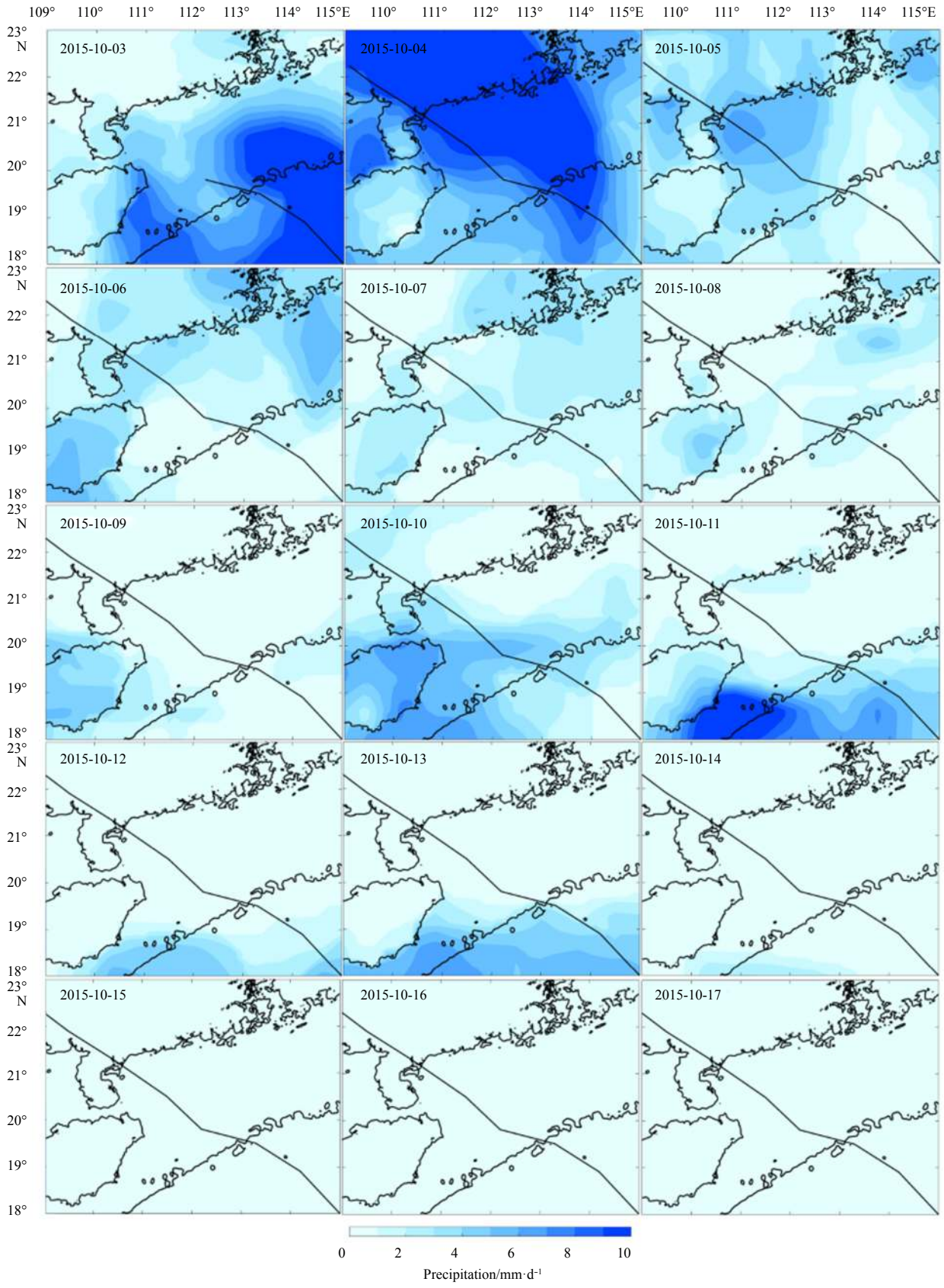

Fig. 5. Time series images of precipitation in the northwestern SCS after the Typhoon Mujigea (2015) passage. Black lines represent the typhoon track. Black contours are isobaths of 200 m. Dates of images read year-month-day.

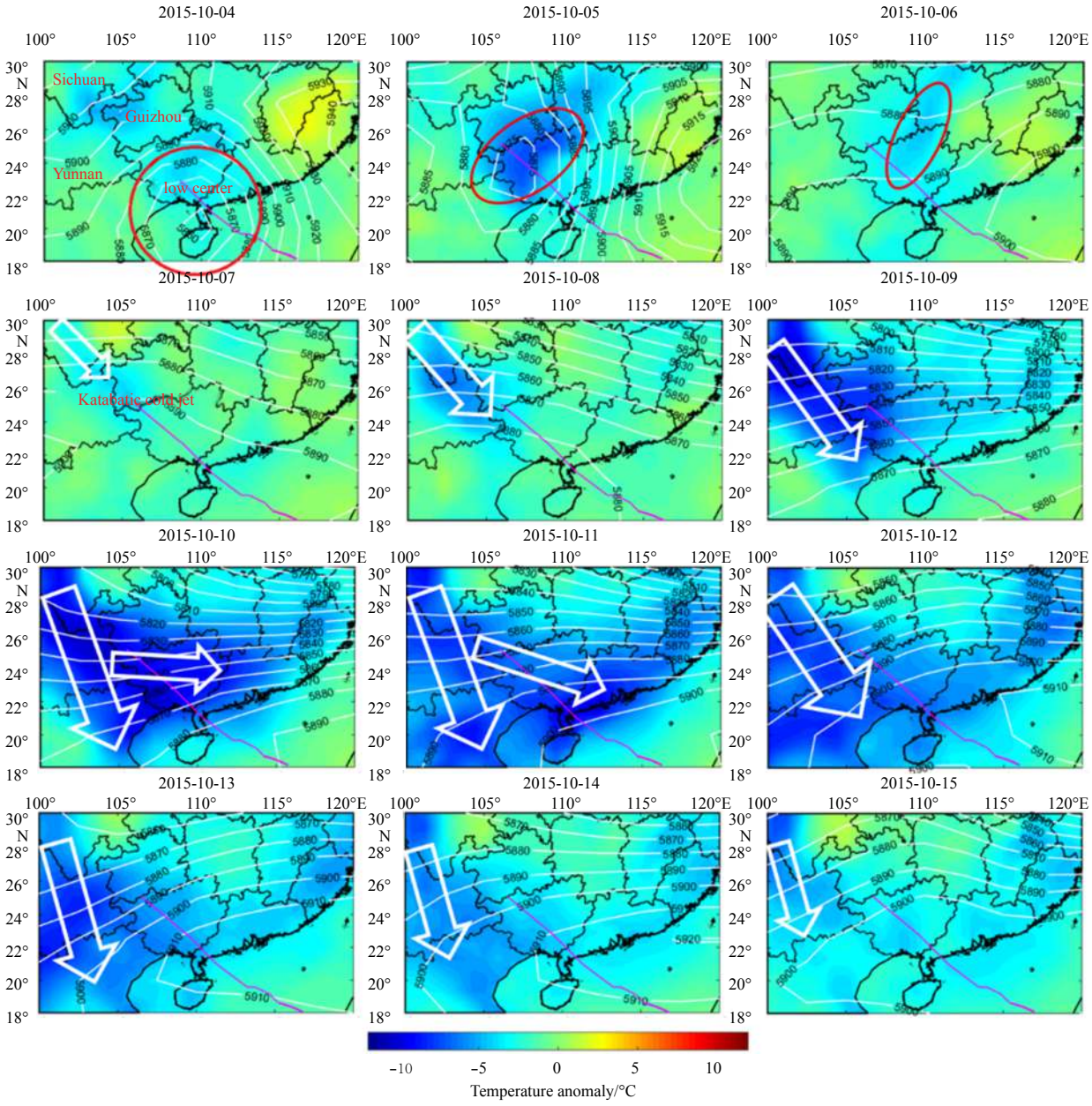

Fig. 6. Time series weather charts of the air temperature anomaly at 2 m (ΔT_{2M}) and the potential height (white contours with numerals in m) at 500 hPa on October 4–15 after Typhoon Mujigea (2015) passage.

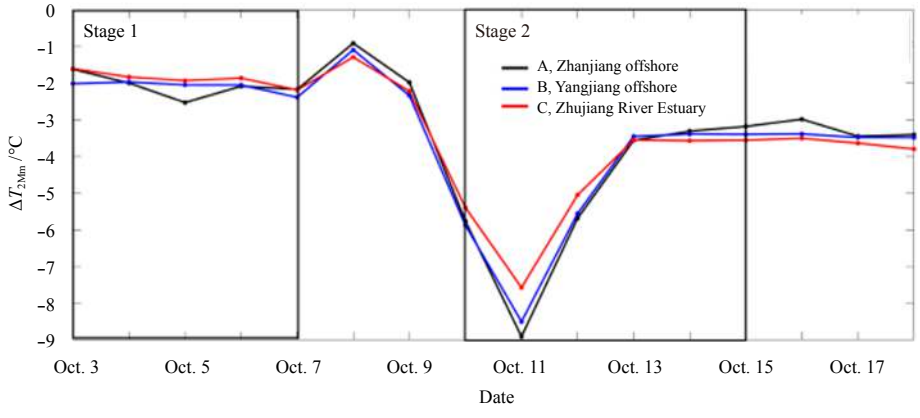

Fig. 7. Variability of the region-averaged sair temperature anomaly at 2 m ΔT2Mm at Stations A, B and C.

lagged behind the air temperature dropping for 4 d.

In order to verify the correlation between the cold air and the extended cooling of SST, we calculate the 4-d lag correlation coefficients between ΔSST_m and ΔT_{2Mm}, since the maximum SST drop occurred 4 d later than the maximum air temperature drop. The results show that ΔSST_m and ΔT_{2Mm} have correlation coefficients of 0.75, 0.82 and 0.75 for Stations A, B and C, respectively, implying that ΔSST_m is highly dependent on ΔT_{2Mm}.

4.4 *SSHA*

Figure 8 shows the SSHA time series images in the study area after Typhoon Mujigea (2015) passage. One can see that there was a negative SSHA center near the coast on the right side of the typhoon track on October 3 and 4, when the typhoon passed over the study area. The negative center moved westward and strengthened on October 5–7, consistent with the SST cooling at the first stage. After October 7, the negative SSHA weakened and disappeared on October 11. From October 12, the SSHA returned back to the climatological features in October, i.e., positive SSHA along the coast with the highest values of about 30 cm near the Zhujiang River Estuary. The SSHA were positive with magnitude increased from about 25 to 35 cm from October 11 to 15, completely unlike the low SSHA from –5 to –40 cm at the first cooling stage, implying that the variation of SSHA did not lead to the extended cooling.

The sea surface current velocity vectors derived from 5-d SODA dataset are also shown in Fig. 8. One can see that there was weak southwestward flow with a magnitude less than 0.1 m/s. The flow directions were consistent with that of the surface wind at the extended cooling stage as shown in Figs 2 and 4. Thus, the water in the northern SCS might be transported southward. However, as shown in Fig. 2, the SST in the northern SCS was unusually higher than that in the study area at the second cooling stage. Thus, the surface current could not bring negative heat flux to contribute to the extended cooling.

In summary, among the atmospheric and oceanic processes, the drop of air temperature is a main mechanism contributing the extended cooling event. Thus, cold air southward intrusion after the disturbance of typhoon will be analyzed in the next section.

5 Typhoon induced cold air southward intrusion

5.1 *Katabatic cold jet*

Typhoon Mujigea (2015) is a super typhoon occurred in local autumn. In this season, cold air develops over the northern Eurasian continent, and the subtropical high (SH) with hot air retreats southward. Between the cold air and the SH, the front of the westerly wind strengthens and favors the cold-air outbreak if meridional flow develops in the zonal wind. The landed typhoon might meet and disturb the westerly wind front, trigger the meridional circulation in the zonal wind, and induce the southward intrusion of cold air (Meng, 1984).

On the large-scale circulation, as shown in the left panels of Fig. 10, the SH (bold-white contour line of 5 880 m) controlled the area south of 30°N before Typhoon Mujigea (2015) landing on October 3, 2015. The front of the westerly wind (dense white contour lines) was zonally distributed at about 30–60°N with its southern edge over the YGP at about 110°E. As the typhoon moved northwestward to the YGP on October 5, it hit the southern edge of the front. Meanwhile, the SH broke into two parts. The low-pressure and positive-vorticity disturbance of typhoon induced the instability of the zonal front. A cyclonic eddy at about 110°E followed by an anticyclonic meander ridge at 80°E developed in the zonal wind on October 7. The eddy and the meander grew in following days, as well as a meridional trough (black curve) within the eddy. Thus, meridional component of winds was enhanced in the westerly. The eddy moved southeastward with the meridional trough slanted zonally. On October 11, the trough was almost zonally distributed. Then, cold air outbreak swapped the south China as the trough transferred from zonal to meridional orientation.

In local small-scale circulation near the QTP and the YGP as shown in the right panels of Fig. 9, one can see that there was southwesterly wind (black arrow) on October 3–5 when Typhoon Mujigea (2015) approaching. As the eddy and meridional flow developed in the westerly with the typhoon-front interaction, the wind on the QTP and YGP turned to be northwesterly on October 7. Such northwesterly wind favored the cold air on the QTP blowing downward and the katabatic cold jet (blue dash circle) formed at the YGP near the typhoon track (magenta line). The northwesterly wind enhanced on October 9. Thus, the cold jet intensified and intruded southeastward to the Biebu Gulf. On October 11, the cold air extended to the Guangdong coast and the air temperature in the study area dropped most. The cold air intrusion weakened on October 12, when the SH retreated back to the YGP and the wind changed to southwesterly. Then, the SST cooled again with the maximum drop of –4°C occurred 4 d later on October 15.

We further revisit recent studies of typhoons in autumn, and find that typhoons Krosa (2007), Bopha (2012) and Lionrock (2016) attracted cold air intrusion. The SST drop for an extended cooling event is then calculated as the daily SST after typhoon passage minus the average SST of 7 d before typhoon entering the coastal ocean. The results indicate that the maximum SST drop reached –5°C.

5.2 *Net air-sea heat flux*

Figure 10 shows the net air-sea heat flux in the study area during the cold air intrusion. The net heat flux is the sum of the solar short-wave heat flux, the net long-wave heat flux, the latent heat flux and the sensible heat flux, of which the data downloaded from ECMWF. One can see that positive values of (1–2)×10^6 J/m^2 dominated the northern SCS on October 7, indicating the heat absorption from the atmosphere (Fig. 10a). On October 9 (Fig. 10b), the Beibu Gulf changed from absorbing the heat to losing the heat, and the net heat flux reduced to –1×10^6 J/m^2, while other regions still absorbed heat. This is consistent with the time and location of cold air intrusion shown in Fig. 6. On October 11 (Fig. 10c), the whole northern SCS lost heat, and the maximum heat loss exceeded –6×10^6 J/m^2. October 11 was also the day when the air temperature dropped sharply in the northern SCS. On October 16 (Fig. 10d), heat absorption from atmosphere appeared in coastal ocean, consistent with the air temperature and SST recovery after the extending cooling stage shown in Figs 2 and 6.

Time series of the net heat flux during the whole process at Stations A–C were shown in Fig. 10e. One can see that the net heat flux loss from October 8 to 15 was consistent with that of the air temperature anomaly ΔT_{2Mm} shown in Fig. 7, implying the significant contribution of air temperature variation to the sea surface heat flux at the second cooling stage. We calculate the total sea surface heat loss ΔQ by accumulating the net heat flux from October 10 to 15 shown in Fig. 10e. The result is –8×10^6 J/m^2, one to two orders smaller than the previous results of heat loss relatively to depth of the 26°C isotherm (~50–100 m) during typhoon passage (Shay et al., 2000; Sun et al., 2012; Jaimes and Shay, 2015). We believe our result is reasonable if considering the

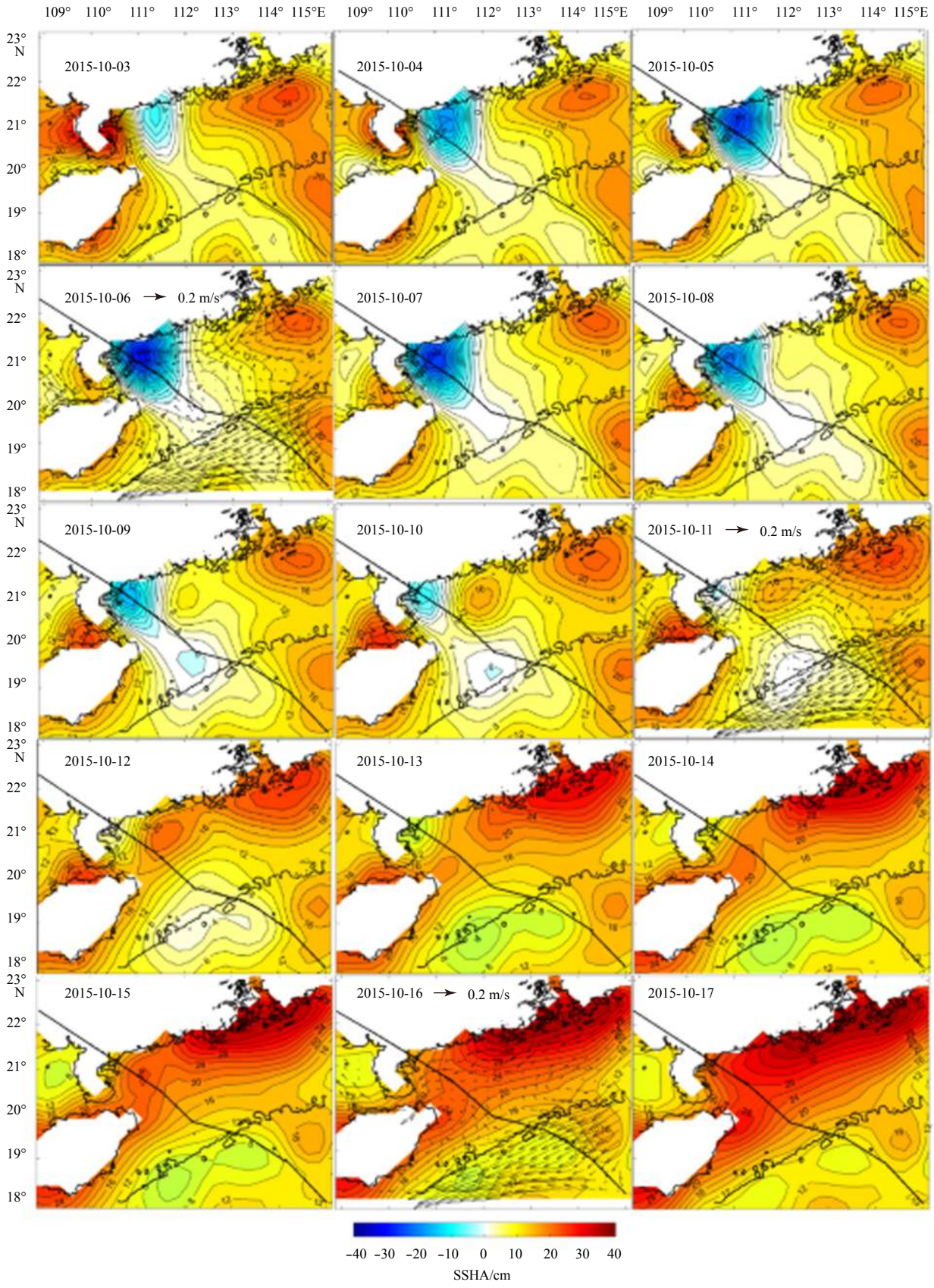

Fig. 8. Time series images of SSHA in the northwestern SCS after the Typhoon Mujigea (2015) passage. Black lines represent the typhoon track. Black contours are isobaths of 200 m. Dates of images read year-month-day. Arrowson October 6,11 and 16 represent the surface current velocity vectors derived from SODA dataset.

different cooling mechanism from the previous investigations. Here, the heat loss was forced by the cold air intrusion and occurred in the near surface layer, while the heat loss during typhoon passage calculated by previous investigators was that in the whole upper layer above 26°C isotherm and supplied the heat to typhoon. In our cases, it is a reasonable estimate that only the top surface 0.5-m water was cooled by the cold air intrusion. According to the Joule's law, the SST cooling ΔSST associated with the heat loss ΔQ is

$$\Delta\mathrm{SST} = \Delta Q/(C_p \times M_\mathrm{a}) = \Delta Q/(C_p \times \rho \times h), \quad (2)$$

where M_a is the water mass per unite area, C_p is the specific heat capacity of the sea water, ρ is the density of the sea surface water, and h is the thickness of the top surface water. Taking ρ= 1.02×10^3 kg/m^3, C_p= 4×10^3 J/(kg·°C), and h = 0.5 m, we have ΔSST = –3.9°C as ΔQ = – 8×10^6 J/m^2. This value is almost identical with the maximum SST cooling of –4°C at the second cooling stage given in previous sections, further indicating the significant contribution of the cold air intrusion and the heat loss to the unusual SST cooling event.

Meanwhile, we find there was no remarkable similarity of the heat flux to $\Delta T_{2\mathrm{Mm}}$ from October 3 to 7, implying the different

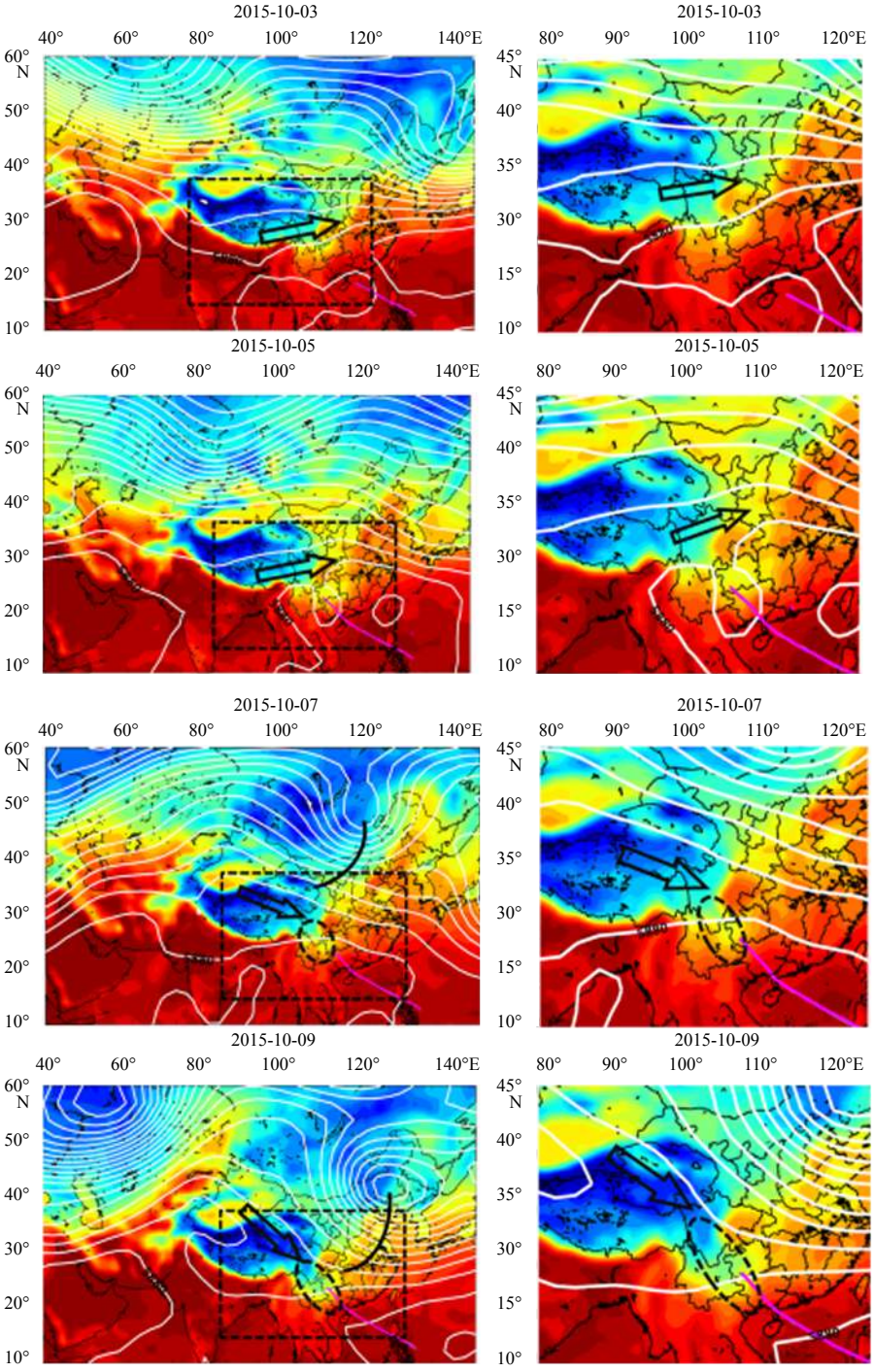

Fig. 9.

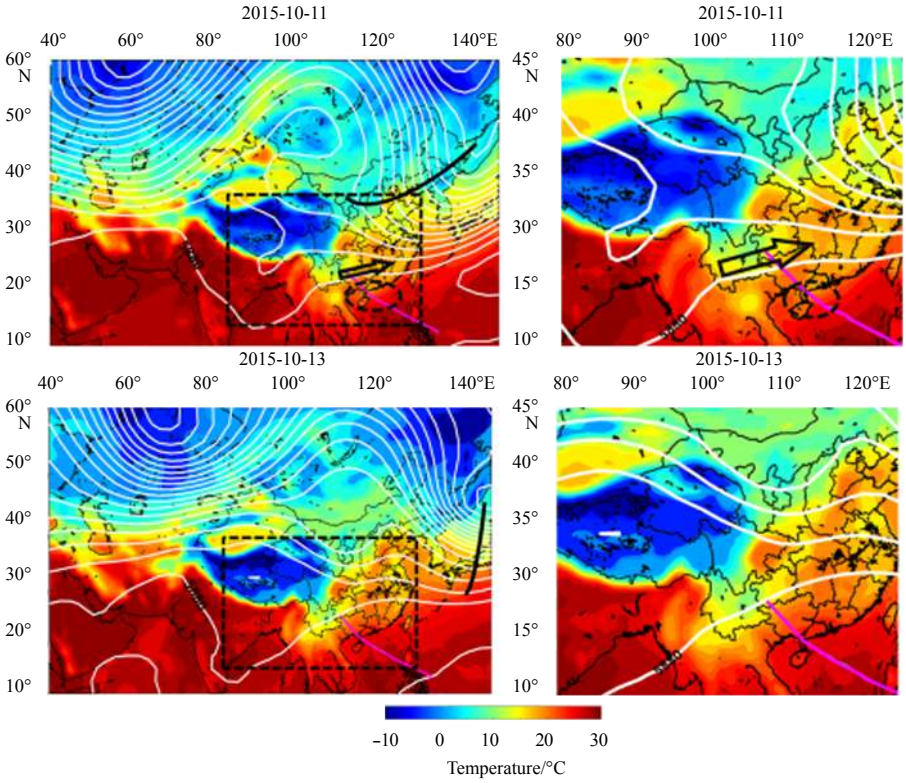

Fig. 9. Variation of the large-scale atmosphere circulation shown by 2-m air temperature and the potential height at 500 hPa (white contours) after Typhoon Mujigea (2015) landed. The bold white contours of 5 880 m represent the subtropical high (SH). The black curve represents the westerly trough. Magenta lines represent the track of Typhoon Mujigea (2015). Dashed black circles represent the cold air intrusion area. Black arrows show the local wind direction.

mechanisms of heat loss at the first stage from the cold air at the second stage. In fact, the SST cooling at the first stage is similar to the typhoon cold wake (D'Asaro et al., 2014). The strong ocean mixing and cold water upwelling directly induced by typhoon play the important roles in the heat loss at the first stage, while the katabatic cold jet induced by landed typhoon dominates the heat loss and SST cooling at the second stage.

6 Discussion

6.1 *Atmospheric or oceanic processes significant for extended cooling event*

The cold wakes after typhoon area generally observed phenomenon in the ocean. The cold anomaly may last for weeks to month before recovery to normal states (D'Asaro et al., 2014). The maximum SST drop of the typhoon wake seldom occurred longer than 7 d after typhoon passage (Dare and McBride, 2011; Yang et al., 2012b). The first cooling event is such a cold wake immediately occurring after typhoon passage and reached a maximum SST drop about 3–4 d later. However, the extend cooling event in the studied case started on the seventh day after typhoon passage, and reached a maximum drop on the twelfth day. The usual extended cooling is different from the cold wake at the first stage, which is attributed to ocean response to typhoon, such as mixing and upwelling (Zhang et al., 2014).

In order to determine the dominant process in the extended cooling event, we analyze both atmospheric and oceanic mechanisms that contribute the ocean surface heat flux in Sections 4 and 5. We find that the atmospheric process of the cold air intrusion dominate in the second cooling stage. Here, the temporal-spatial scale analysis provides further evidence to determine the significant oceanic and atmospheric processes. For the time scale, as shown in Fig. 3, there were 7 d from the typhoon passing the northwestern SCS on October 3 to the beginning of the extended SST cooling on October 10, and 12 d to the maximum SST drop on October 15. This is much longer than a 2–3 d time lag of the coastal ocean cooling response to the typhoon passage. On the other hand, the extended SST cooling occurred 4 d after the air temperature drop. This lag time is consistent with that of the ocean response to atmospheric process. For the spatial scale, as shown in Fig. 2, the extended SST cooling spread from the coastal water to the continental shelf area. The coverage of the extended cooling is larger than that covered by the typhoon, and the maximum SST drop is also larger than that at the first stage after typhoon passage. These phenomena imply that there is a large-scale and powerful atmospheric process from the land, rather than the local oceanic processes, having major contribution to the second cooling event. The air temperature drops associated with a katabatic cold jet are thus found to be a dominant mechanism responsible to the extended SST cooling event.

6.2 *Typhoon-westerly interaction and katabatic cold jet formation*

In Section 5, we attribute the cold air intrusion inducing the extended SST cooling event to the interaction of typhoon with the westerly front and the associated katabatic cold jet from the QTP and the YGP.

In fact, previous investigators have analyzed the role of typhoon interacting with the westerly in the cold air outbreaks.

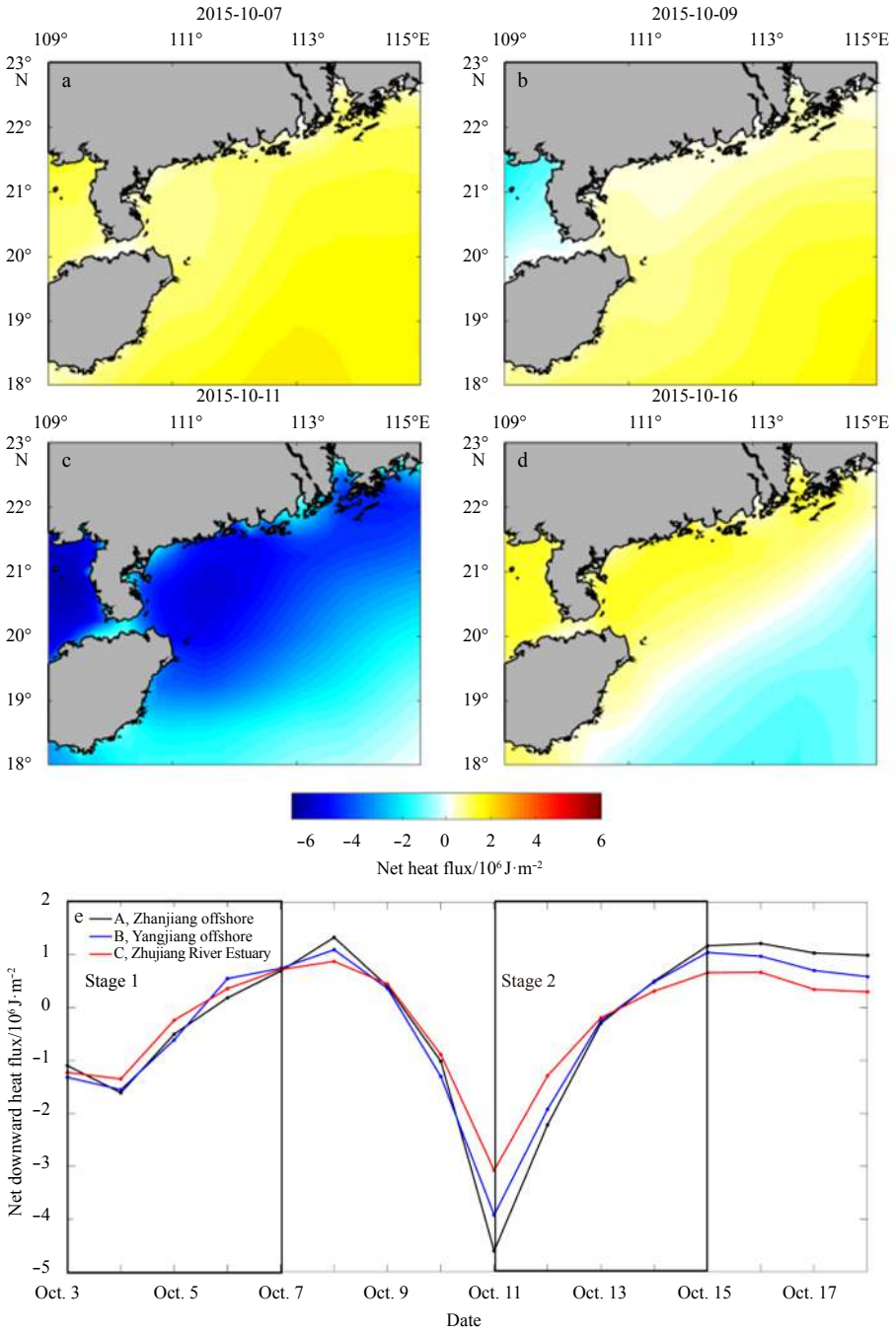

Fig. 10. Time series of net heat flux after the Typhoon Mujigea (2015) passage (a–d), and temporal variability of the regional mean net heat flux at Stations A, B and C (e).

Meng et al. (1983) statistically analyzed the historical typhoons entering Guangxi, China in September and October from 1958 to 1990. They found 16 of total 23 typhoons induced cold dew. Meng (1984) presented that the northwestward typhoon in the SCS in autumn could attract the cold air southward intrusion, when typhoon met the westerly trough. Hu (1989) theoretically analyzed the effects of typhoon on the East Asian circulation in autumn. They suggested that the typhoon is a medium that transfers the energy in the low latitudes to the westerly, reducing the zonal wind in the westerly, enhancing the meridional circulation, and thus inducing southward intrusion of cold air. Zhou and Ren (1992) also found that the enhanced eddy energy by typhoon helps the cold air accelerating southward. In recent years, researchers investigated the co-effects of autumn typhoon and cold air on precipitation (Chen et al., 2017). The numerical simulation by Wang et al. (2017) showed that the mid-latitude circulation will be more meridional if typhoon strongly interacts with the westerly trough.

In this study, the weather charts clearly show that cyclonic eddy and anticyclonic meander as well as trough and ridge developed in the westerly after Typhoon Mujigea (2015) approaching the southern edge of the westerly front near the YGP. As a consequence, meridional circulation strengthened, and the cold air in the north intruded southward behind the westerly trough.

What is more, the developed northwesterly wind and over the QTP and the YGP led the cold air on the QTP downward as a katabatic cold jet intensively intruding southeastward to the northern SCS. If focusing on the pathway of the cold jet intrusion as shown in Fig. 6, one can see that both the cold jet and the typhoon go through the same air flow corridor approximately along Guangxi, Yunnan, and Guizhou, and the typhoon track is on the right and the cold jet on the left. It seems that this corridor is the pathway for exchange of warm-humidity air from the ocean by the typhoon and the cold-dry air from the QTP by the cold jet. The cold jet seems to be a cold typhoon from the land as the feedback of the atmosphere to the landed typhoon from the ocean, and plays important role in the extended cooling of the coastal ocean. The detailed dynamics of typhoon-westerly interaction and katabatic cold jet worth further pursing in the further research.

7 Conclusions

Using multiple satellite data and weather charts from October 3 to 18, 2015, this study analyzes a new phenomenon of unusual coastal ocean cooling event associated with typhoon Mujigea (2015) passing the northwestern SCS. Mechanisms of the unusual SST cooling event associated with the wind, precipitation, air temperature, surface current, and SSHA are analyzed. The major findings are summarized as follows:

(1) A second coastal cooling event suddenly occurred on October 10 after three-day recovery from the first cooling event starting on October 3, 2015 immediately after typhoon passage. This unique extended cooling event lasted for 5 d, and reached a maximum SST drop of –4°C on October 15, which had been 12 d later since the typhoon passage on October 3, 2015.

(2) The cold air intrusion of a katabatic cold jet lead to the unusual cooling event. The air temperature sharply dropped in advance of the second SST cooling event, and contributed most to the ocean heat loss. The maximum air temperature drop reached –9°C on October 11, 2015, and the maximum SST drop occurred 4 d later. The lagged correlation coefficient of the air temperature drop and the SST drop reached 0.8.

(3) The landed typhoon disturbed the westerly front and triggered meridional air flow and low-pressure trough, so that the katabatic cold jet intruded downward from the QTP, passed through the YGP and moved to the coastal ocean of the northwestern SCS. It is this cold air feedback to typhoon cools the SST again after the first cooling occurring immediately after the typhoon passage.

References

Allahdadi M N, Li Chunyan. 2018. Numerical simulation of Louisiana shelf circulation under hurricane Katrina. Journal of Coastal Research, 34(1): 67–80, doi: 10.2112/JCOASTRES-D-16-00129.1

Black W J, Dickey T D. 2008. Observations and analyses of upper ocean responses to tropical storms and hurricanes in the vicinity of Bermuda. Journal of Geophysical Research, 113(C8): C08009, doi: 10.1029/2007JC004358

Chen Peng, Pang Yue, Zhang Hong, et al. 2017. Analysis of the"9.17" heavy rainfall in Chongqing under the influence of the typhoon and cold air. Torrential Rain and Disasters, 36(3): 227–234

Chiang T L, Wu C R, Oey L Y. 2011. Typhoon Kai-Tak: An ocean' sperfect storm. Journal of Physical Oceanography, 41(1): 221–233, doi: 10.1175/2010JPO4518.1

Cione J J, Uhlhorn E W. 2003. Sea surface temperature variability in hurricanes: Implications with respect to intensity change. Monthly Weather Review, 131(8): 1783–1796, doi: 10.1175//2562.1

D'Asaro E A, Black P G, Centurioni L R, et al. 2014. Impact of typhoons on the ocean in the Pacific. Bulletin of the American Meteorological Society, 95(9): 1405–1418, doi: 10.1175/BAMS-D-12-00104.1

D'Asaro E A, Sanford T B, Niiler P P, et al. 2007. Cold wake of hurricane Frances. Geophysical Research Letters, 34(15): L15609

Dare R A, McBride J L. 2011. Sea surface temperature response to tropical cyclones. Monthly Weather Review, 139(12): 3798–3808, doi: 10.1175/MWR-D-10-05019.1

Glenn S M, Miles T N, Seroka G N, et al. 2016. Stratified coastal ocean interactions with tropical cyclones. Nature Communications, 7: 10887, doi: 10.1038/ncomms10887

Hu Jian. 1989. Effects of recurving typhoon activity on the variations of autumnal circulation over East Asia. Chinese Journal of Atmospheric Sciences, 13(3): 305–312

Jaimes B, Shay L K. 2015. Enhanced wind-driven downwelling flow in warm oceanic eddy features during the intensification of Tropical Cyclone Isaac (2012): Observations and theory. Journal of Physical Oceanography, 45(6): 1667–1689, doi: 10.1175/JPO-D-14-0176.1

Kuo Yichun, Lee Ming'an, Chern C S. 2014. Typhoon-induced ocean responses off the southwest coast of Taiwan. Ocean Dynamics, 64(11): 1569–1581, doi: 10.1007/s10236-014-0776-8

Lai Qiaozhen, Wu Liguang, Shie C L. 2013. Sea surface temperature response to typhoon Morakot (2009) and the influence on its activity. Journal of Tropical Meteorology, 29(2): 221–234

Liang Xiaohong, Ge Lili. 2014. Analysis of impacts of typhoons on sea surface temperature of coastal region of Jiangsu Province. Journal of Aquaculture, 35(10): 37–42

Lin I I, Chan J C L. 2015. Recent decrease in typhoon destructive potential and global warming implications. Nature Communications, 6: 7182, doi: 10.1038/ncomms8182

Lin I I, Liu W T, Wu C C, et al. 2003. New evidence for enhanced ocean primary production triggered by tropical cyclone. Geophysical Research Letters, 30(13): 1718

Liu Shanshan, Sun Liang, Wu Qiaoyan, et al. 2017. The responses of cyclonic and anticyclonic eddies to typhoon forcing: The vertical temperature-salinity structure changes associated with the horizontal convergence/divergence. Journal of Geophysical Research, 122(6): 4974–4989

Liu Zenghong, Xu Jianping, Sun Chaohui, et al. 2014. An upper ocean response to Typhoon Bolaven analyzed with Argo profiling floats. Acta Oceanologica Sinica, 33(11): 90–101, doi: 10.1007/s13131-014-0558-7

Meng Yuanwen. 1984. The effect of typhoon on the southward movement of cold air. Journal of Tropical Meteorology, (1): 84–89

Meng Yuanwen, Wu Rencai, Jiang Boren. 1983. The role of typhoon in the process of cold dew. Journal of Guangxi Meteorology, (4): 1–4

Nelson N B. 1996. Cover the wake of hurricane Felix. International Journal of Remote Sensing, 17(15): 2893–2895, doi: 10.1080/01431169608949116

Pan Jiayi, Sun Yujuan. 2012. Estimate of ocean mixed layer deepening after a typhoon passage over the South China Sea by using satellite data. Journal of Physical Oceanography, 43(3): 498–506

Price J F. 1981. Upper ocean response to a hurricane. Journal of Physical Oceanography, 11(2): 153–175, doi: 10.1175/1520-0485(1981)011<0153:UORTAH>2.0.CO;2

Price J F, Morzel J, Niiler P P. 2008. Warming of SST in the cool wake of a moving hurricane. Journal of Geophysical Research, 113(C7): C07010

Shan Haixia, Guan Yuping, Huang Jianping. 2014. Investigating different bio-responses of the upper ocean to Typhoon Haitang using Argo and satellite data. Chinese Science Bulletin, 59(8): 785–794, doi: 10.1007/s11434-013-0101-9

Shang Shaoling, Li Li, Sun Fengqin, et al. 2008. Changes of temperature and bio-optical properties in the South China Sea in response to Typhoon Lingling, 2001. Geophysical Research Letters, 35(10): L10602

Shay L K, Goni G J, Black P G. 2000. Effects of a warm oceanic feature on Hurricane Opal. Monthly Weather Review, 128(5): 1366–1383, doi: 10.1175/1520-0493(2000)128<1366:

EOAWOF>2.0.CO;2

Shi Yuxin, Xie Lingling, Li Mingming, et al. 2017. Impacts of Typhoon Mujigea on sea surface temperature and chlorophyll-a concentration in the coastal ocean of western Guangdong. Journal of Guangdong Ocean University, 37(3): 49–58

Stewart R H. 2008. Introduction to Physical Oceanography. Texas: Texas A&M University, 51–52

Sun Liang, Yang Juanjian, Xian Tao, et al. 2012. Ocean responses to Typhoon Namtheun explored with Argo floats and multiplatform satellites. Atmosphere Ocean, 50(Sup1): 15–26, doi: 10.1080/07055900.2012.742420

Tsai Y, Chern C S, Wang J. 2008. The upper ocean response to a moving typhoon. Journal of Oceanography, 64(1): 115–130, doi: 10.1007/s10872-008-0009-1

Tsai Y, Chern C S, Wang J. 2012. Numerical study of typhoon-induced ocean thermal content variations on the northern shelf of the South China Sea. Continental Shelf Research, 42: 64–77, doi: 10.1016/j.csr.2012.05.004

Walker N D, Leben R R, Balasubramanian S. 2005. Hurricane-forced upwelling and chlorophyll a enhancement within cold-core cyclones in the Gulf of Mexico. Geophysical Research Letters, 32(18): L18610

Wang Xidong, Liu Hailong, Foltz G R. 2017. Persistent influence of tropical North Atlantic wintertime sea surface temperature on the subsequent Atlantic hurricane season. Geophysical Research Letters, 44(15): 7927–7935, doi: 10.1002/2017GL074801

Wang Guihua, Su Jilan, Ding Yihui, et al. 2007. Tropical cyclone genesis over the South China Sea. Journal of Marine Systems, 68(3–4): 318–326, doi: 10.1016/j.jmarsys.2006.12.002

Webster P J, Hollan G J, Curry J A, et al. 2005. Changes in tropical cyclone number, duration, and intensity in a warming environment. Science, 309(5742): 1844–1846, doi: 10.1126/science.1116448

Wentz F J, Gentemann C, Smith D, et al. 2000. Satellite measurements of sea surface temperature through clouds. Science, 288(4567): 847–850

Xie Lingling, He Chaofeng, Li Mingming, et al. 2017. Response of sea surface temperature to typhoon passages over the upwelling zone east of Hainan Island. Advances in Marine Science, 35(1): 8–19

Xu Wenling, Su Jie. 2007. The impact of typhoons on sea surface temperature in the Western North Pacific Ocean. Periodical of Ocean University of China, 37(S2): 17–22

Yang Bing, Hou Yijun. 2014. Near-inertial waves in the wake of 2011 Typhoon Nesat in the northern South China Sea. Acta Oceanologica Sinica, 33(11): 102–111, doi: 10.1007/s13131-014-0559-6

Yang Jianyuan, Sun Liang, Duan Anmin, et al. 2012a. Impacts of the binary typhoons on upper ocean environments in November 2007. Journal of Applied Remote Sensing, 6(1): 063583

Yang Lei, Wang Dongxiao, Peng Shiqiu. 2012b. Comparison between MM5 simulations and satellite measurements during Typhoon Chanchu (2006) in the South China Sea. Acta Oceanologica Sinica, 31(2): 33–44, doi: 10.1007/s13131-012-0190-3

Zhang Han, Chen Dake, Zhou Lei, et al. 2016. Upper ocean response to typhoon Kalmaegi (2014). Journal of Geophysical Research, 121(8): 6520–6535

Zhang Shuwen, Xie Lingling, Zhao Hui, et al. 2014. Tropical storm-induced turbulent mixing and chlorophyll-*a* enhancement in the continental shelf southeast of Hainan Island. Journal of Marine Systems, 129: 405–414, doi: 10.1016/j.jmarsys.2013.09.002

Zheng Zhewen, Ho C R, Kuo N J. 2008. Importance of pre-existing oceanic conditions to upper ocean response induced by Super Typhoon Hai-Tang. Geophysical Research Letters, 35(20): L20603, doi: 10.1029/2008GL035524

Zheng Zhewen, Ho C R, Zheng Quanan, et al. 2010. Satellite observation and model simulation of upper ocean biophysical response to Super Typhoon Nakri. Continental Shelf Research, 30(13): 1450–1457, doi: 10.1016/j.csr.2010.05.005

Zheng Quanan, Lai R L, Huang N E, et al. 2006. Observation of ocean current response to 1998 Hurricane Georges in the Gulf of Mexico. Acta Oceanologica Sinica, 25(1): 1–14

Zhou Xuequn, Ren Chong. 1992. Effects of autumn recurving typhoon in northwestern Pacific on the cold air over the South China Sea. Marine Forecasts, 9(2): 74–78